

Dirac and nodal-line magnons in collinear antiferromagnets

Kangkang Li,^{1,2,*} Chenyuan Li,^{3,*} Jiangping Hu,^{1,4} Yuan Li,^{3,4,†} and Chen Fang^{1,‡}

¹*Beijing National Laboratory for Condensed Matter Physics,
and Institute of Physics, Chinese Academy of Sciences, Beijing 100190, China*

²*University of Chinese Academy of Sciences, Beijing 100049*

³*International Center for Quantum Materials, School of Physics, Peking University, Beijing 100871, China*

⁴*Collaborative Innovation Center of Quantum Matter, Beijing 100871, China*

We study the topological properties of magnon excitations in three-dimensional collinear antiferromagnets, where the ground state configuration is invariant under space-time-inversion, a composite magnetic-group symmetry of time-reversal followed by space inversion. We prove in these systems that Dirac points and nodal lines are symmetry-protected at band crossing between optical magnon branches, in the presence and the absence, respectively, of the conservation of the total spin along the ordered moments. As a concrete example, we study a Heisenberg spin model for a “spin-web” compound, Cu_3TeO_6 , and show the presence of the Dirac magnons using linear spin wave approximation. The corresponding topological surface states are calculated, which exhibit “double-arcs” for the equal energy contours on the surface.

I. INTRODUCTION

The theoretical proposal^{1,2} and experimental discovery^{3–5} of Weyl semimetals have opened up a new research field called topological semimetals⁶. Due to the topologically nontrivial structure of wavefunctions, near a positive Weyl point, the electronic spin polarizations take on an “all-out” configuration, making the Weyl point a magnetic monopole in momentum space. Physically, the essence of topological band theory, that the Bloch wavefunction on a closed surface in momentum space can have nontrivial topological structures, is independent of the statistics of the constituent particles^{7–9}. By replacing the electronic spin polarization in the above example by light polarization, for instance, one obtains a topological band crossing in photonic crystals. Such ideas of generalization have inspired researchers to find topologically nontrivial band crossings in boson systems of photons¹⁰, phonons¹¹ and magnons¹².

Most topological band crossings studied so far are protected by lattice symmetries: Weyl points by (lattice) translation symmetry, Dirac points by translation and point-group or nonsymmorphic symmetries^{13–17}, and other exotic band degeneracies at Brillouin-zone boundary^{18–22} by certain space group symmetries. An (almost) full classification of these band crossings has appeared in the literature^{23,24}. In this paper, we focus on a new type of symmetry groups: the magnetic groups, which naturally rise in magnetically ordered systems. The difference between a magnetic group and a space group is that in addition to lattice symmetries, the former generically contains elements of the form ST , where S is some space-group operation and T time-reversal²⁵. Band crossings protected by magnetic groups can presumably be found in the electronic band structures in magnetic materials, as well as the band structure of magnons (coherent spin excitations) over a magnetic ground state.

In this paper, we choose for our study one of the simplest magnetic groups, generated by PT , where P is spa-

tial inversion. This magnetic group pertains to various antiferromagnets with centro-symmetric crystal lattices, where two spins related by inversion have opposite polarizations in the ordered state. In addition, we require that the ordered moments are collinear, introducing a global $U(1)$ spin-rotation symmetry along the ordered moments. Then, if the spin interactions are either fully isotropic such as Heisenberg [with $SU(2)$ spin-rotation symmetry], or have an easy axis [with $U(1)$ spin-rotation symmetry], we show that Dirac points are protected in the band structure of the magnons. The excitations near such Dirac points in the magnon bands are hence called Dirac magnons. Different from all known types of Dirac points, these Dirac points are *not* pinned to any high-symmetry points¹³, lines^{14,15,17} or planes, but can appear at generic momenta in the magnetic Brillouin zone. On the surface, in the region near the projection of a Dirac point in the surface Brillouin zone, there are topological surface states, whose dispersion takes on the shape of a “double-helicoi”¹⁷, and the equal energy contours are “double arcs”^{15,17,26} connecting the projections of two Dirac points. Furthermore, we find that when the $U(1)$ symmetry is broken (*e.g.*, by Dzyaloshinsky-Moriya interactions^{27,28} or other anisotropic effects), but PT still preserved, each Dirac point *necessarily* breaks into a nodal ring. In Ref.[29], it was proved that nodal lines protected by $(PT)^2 = 1$ can be divided into two types, both protected by the π -Berry phase^{29–33}, but are distinguished by the presence (absence) of the Z_2 -monopole charge, and the second latter type have not been predicted in realistic materials³⁴. Here we prove that every nodal ring broken from a Dirac point upon $U(1)$ -symmetry breaking has nontrivial Z_2 -charge.

To be concrete, we apply the general theory to a three-dimensional spin-web compound, Cu_3TeO_6 , which develops long-range collinear antiferromagnetic order below $T_N \approx 61$ K. We use a J_1 - J_2 ($J_1 > J_2 > 0$) Heisenberg model to simulate the spin interactions and calculate the magnon band structure using linear-spin-wave approximation, where eight pairs of Dirac points are identified

between two optical magnon branches. Surface states on the (001)- and (111)-planes are simulated and in both cases we find equal energy contours take the form of “double-arcs” connecting the projections of the Dirac points. Experiments for detecting key features of Dirac and nodal line magnons are proposed.

II. GENERAL THEORY

We begin by noting that when the total S_z is preserved, all single-particle excitations can be labeled by their spin quantum numbers. For magnons, these numbers are $+1$ and -1 , and magnons with opposite spins are decoupled. Next we look at how the magnetic-group symmetry PT acts on the magnons. Physically, parity (spatial-inversion) preserves spin and time-reversal reverses it, making the composite symmetry PT invert the spin quantum number of a magnon. Based on these observations, we see that the single-particle Hamiltonian decouples into two sectors, one for each spin quantum number, or symbolically

$$H = H_+ \oplus H_-, \quad (1)$$

where H_{\pm} is the Hamiltonian for the spin- ± 1 sector in the spin system. Magnetic group symmetry PT then requires

$$H_+ = H_-^*. \quad (2)$$

There is no further constraint on the form of H_+ except that it is hermitian. When H_+ is defined in three-dimensional Brillouin zone, there can be Weyl points in the spectrum as band crossings¹. Due to Eq. (2), H_- and H_+ have the same band structure and therefore when Weyl points appear in H_+ , there must be Weyl points in H_- . Moreover, since PT reverses the Berry curvature while preserving the momentum, it reverses the monopole charge of a Weyl point. In the end, for each Weyl point in H_+ , there is an equal and opposite Weyl point in H_- at the same momentum, and they together make a Dirac point.

Below are some basic properties of these Dirac points in the bulk. (i) The Weyl points in H_+ are not pinned to any high-symmetry point, line or plane, so the Dirac point may appear at any momentum in the Brillouin zone, in contrast to previously studied Dirac points that are pinned to high-symmetry points and lines. (ii) Since the Weyl points in H_+ must appear in pairs, so do the Dirac points. (iii) Upon PT -symmetry breaking a Dirac point splits into two Weyl points, because in this case $H_- \neq H_+^*$. (iv) For each Dirac point we can define a monopole charge that equals the monopole charge of the Weyl point in H_+ , and two Dirac points with opposite monopole charges “annihilate” each other when they meet in the Brillouin zone, creating a gap.

Due to the bulk-edge correspondence, the topological nature of a bulk node is also manifested on the surface.

For example, a Weyl point in the bulk corresponds to helical surface states near the projection of the bulk node in the surface Brillouin zone^{2,17}. A Dirac point, considered as a superposition of two opposite Weyl points from H_{\pm} respectively, then corresponds to double-helical surface states^{14,17,26}. Due to PT , the dispersions on opposite surfaces are identical.

In realistic magnetic materials, besides the isotropic Heisenberg terms, other terms, such as site-dependent single-ion anisotropy, exchange anisotropy and Dzyaloshinsky-Moriya interaction, break the $U(1)$ spin-rotation symmetry, but will leave the space-time symmetry PT intact. For example, when the bonds connecting two magnetic atoms to the ligand atom make an angle less than 180° , Dzyaloshinsky-Moriya interaction is in general present. When $U(1)$ symmetry is broken, a Dirac point is no longer stable, and as long as PT is still preserved, Weyl points are disallowed¹, so in principle a Dirac point can either be fully gapped or broken into a nodal ring. Further analysis rules out the former possibility, and shows that each Dirac point becomes a nodal ring upon turning on these anisotropic perturbations, where the two bands cross along a one-dimensional closed line.

To see this, we first notice that the spin-lattice coupling does not break the magnetic-group symmetry PT , and that in any spin system $(PT)^2 = +1$. In an earlier theoretical work, one of us showed that in the presence of PT with $(PT)^2 = +1$, the generic band crossing is a nodal ring, which may or may not carry a Z_2 monopole charge – a topological index defined on a sphere enclosing the ring. When a nodal ring carries (does not carry) a Z_2 monopole charge, the ring cannot (can) continuously shrink to a point and disappear. To compute this Z_2 charge, we notice that near the Dirac point, the effective Hamiltonian ($k \cdot p$) is generally given by, up to a gauge

$$H(\mathbf{q}) = q_x \Sigma_{0x} + q_y \Sigma_{zy} + q_z \Sigma_{0z}, \quad (3)$$

where $\Sigma_{\mu\nu} \equiv \sigma_\mu \otimes \sigma_\nu$ and $PT = K \Sigma_{x0}$. In Ref.[29], the Z_2 -index of this Hamiltonian is found to be nontrivial, *i. e.*, the Dirac point is only a special case of a nodal ring when $U(1)$ -symmetry is broken. To our best knowledge, while nodal rings without Z_2 monopole charge have been proposed in many fermionic and bosonic systems³⁴, nodal rings carrying nontrivial Z_2 monopole charge have not yet been predicted in realistic materials.

III. DIRAC MAGNONS IN Cu_3TeO_6

Three-dimensional collinear antiferromagnets are the best platform for us to realize these topological band crossings in k -space and here we have chosen Cu_3TeO_6 , which was recently reported to host a novel spin lattice³⁵, dubbed a three-dimensional spin web^{36,37}. The lattice consists of almost planar Cu^{2+} hexagons that are perpendicular to one of the four space diagonals of the cubic

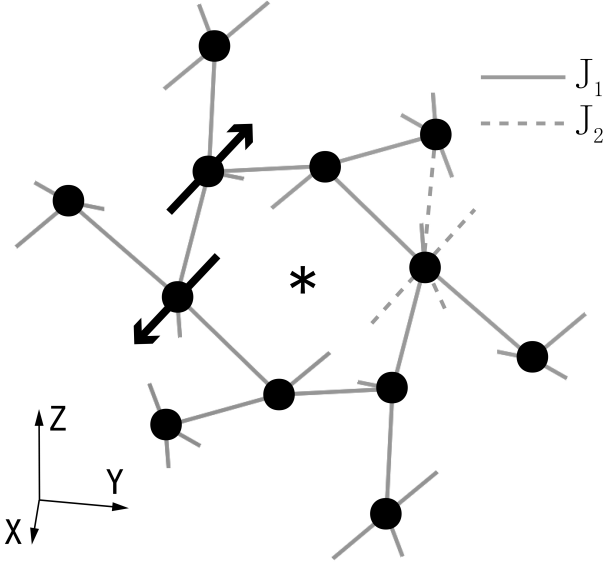


FIG. 1. The Cu^{2+} sublattice and magnetic structure of Cu_3TeO_6 in a primitive cell. Nearest neighbors are connected by solid lines and their spins are antiparallel. Next-nearest neighbors are connected by dotted lines (only one is shown). Star symbol indicates inversion center.

unit cell (Fig. 1), featuring a hybrid between a 3D spin-1/2 network and a low connectivity of the superexchange pathways: each Cu^{2+} ion is shared by two hexagons and has only four nearest neighbors. Below $T_N \approx 61$ K, the system develops long-range antiferromagnetic order that leaves clear signatures in magnetic susceptibility and neutron diffraction measurements³⁵. Without loss of generality, we believe that the large yet highly symmetric magnetic unit cell of Cu_3TeO_6 is favorable for symmetry-protected magnon band crossings in the bulk that inevitably lead to interesting surface states.

Furthermore, We note that the lattice structure of Cu_3TeO_6 is very similar to those of C -type sesquioxides $R_2\text{O}_3$ ($R = \text{Y}, \text{Sc}, \text{In}$, or rare-earth elements)³⁸. The spin lattice of Cu_3TeO_6 can be realized in the latter, if the Wyckoff $24d$ and $8a$ sites can be occupied by magnetic and non-magnetic ions, respectively. Given the rather broad distribution of the R^{3+} ionic radii, ranging from 81 pm (Sc and In) to 106 pm (La), it might be possible to synthesize solid solutions of them, such as Nd_3ScO_6 , with minimal inter-site disorder³⁹. Along with the rich magnetic properties of rare-earth elements, this renders our analysis of Cu_3TeO_6 potentially applicable to a large family of interesting magnetic materials.

Available neutron diffraction data are consistent with a collinear antiferromagnetic spin configuration plotted in Fig. 1, though a slightly noncollinear configuration cannot be completely ruled out³⁵. This ground state is mostly easily understood by assuming the unfrustrated nearest-neighbor Heisenberg exchange interaction $J\mathbf{S}_i \cdot \mathbf{S}_j$. Yet, due to the geometric configuration of the atoms, the next-nearest-neighbor exchange may also have an appreciable

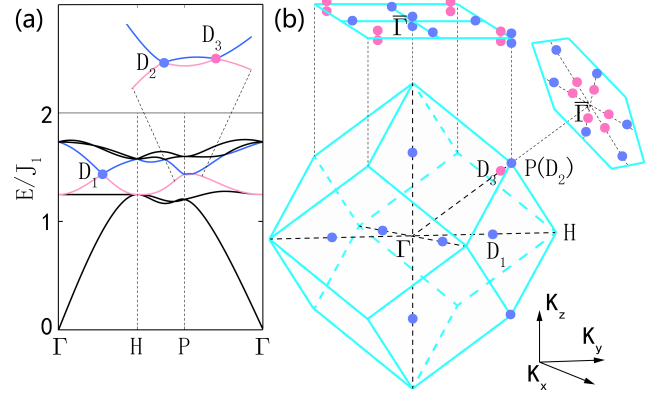


FIG. 2. (a) A typical band structure of the spin-wave dispersion along high-symmetry lines with $J_2 = 0.134J_1 > 0$, where the inset shows a zoomed-in region near P. (b) Positions of all Dirac points in the first Brillouin zone and their projections onto the (001)- and (111)-surface Brillouin zones. Red and blue colors indicate the monopole charge of +1 and -1, respectively. For clarity, only one of the eight W_3 points is displayed in the three-dimensional Brillouin zone in (b).

magnitude, whose sign is likely to be also positive (antiferromagnetic). We thus model the spin interactions in Cu_3TeO_6 using the following J_1 - J_2 Heisenberg model

$$H = J_1 \sum_{\langle ij \rangle} \mathbf{S}_i \cdot \mathbf{S}_j + J_2 \sum_{\langle\langle ij \rangle\rangle} \mathbf{S}_i \cdot \mathbf{S}_j. \quad (4)$$

The classical ground state of H depends on the relative magnitude of J_1 and J_2 , and when $J_2 < J_c = J_1/3$, the ground state configuration matches the experimental one shown in Fig. 1. It is easy to check that this spin configuration preserves both PT and S_z , and hence it may host Dirac magnons. The strongly localized moment, and the relatively small quantum fluctuation in three dimensions allow us to treat the magnon excitations using the linear spin-wave approximation. There are twelve spins in each primary cell, with six pointing downward and six upward in the ground state. (Note that the magnetic order does not enlarge the lattice unit cell.) We perform the standard Holstein-Primakoff transformation on the up spins

$$S_x = \sqrt{\frac{S}{2}}(a + a^\dagger), S_y = -i\sqrt{\frac{S}{2}}(a - a^\dagger), S_z = S - a^\dagger a, \quad (5)$$

and down spins

$$S_x = -\sqrt{\frac{S}{2}}(b + b^\dagger), S_y = -i\sqrt{\frac{S}{2}}(b - b^\dagger), S_z = -S + b^\dagger b. \quad (6)$$

We remark that under spin rotation along z -axis through θ , spin wave operator a transforms as $a \rightarrow ae^{-i\theta}$ on up spins and $b \rightarrow be^{-i\theta}$ on down spins, making them $S_z = +1$ and -1 operators, respectively. All spin-wave operators can thus be divided into two sets by their spins: $\{a, b^\dagger\}$ having $S_z = +1$ and $\{a^\dagger, b\}$ having $S_z = -1$. As

long as the U(1) symmetry is present, these two sets do not couple to each other in a quadratic spin wave Hamiltonian.

For $J_2 = 0.134J_1$ (but see Appendix B for other values of J_2), the magnon bands along high-symmetry lines in the Brillouin zone are plotted in Fig. 2(a). Distinct linear band crossings can be found between two optical branches (marked blue and red). Calculation of the monopole charge using the Wilson loop technique confirms that all these band crossings are Dirac points defined in this paper: there are six positive Dirac points along ΓH and its symmetry equivalents (denoted by D_1), two negative Dirac points at two P's (D_2) and eight negative Weyl points along ΓP and its symmetry equivalents (D_3). More detailed search shows that there is no other band crossing between the two branches.

We remark that the limited experimental data in the literature on this compound cannot fully justify the J_1 - J_2 model (or any spin model), so that some Dirac points may appear away from the positions predicted in our calculation. Nonetheless, we emphasize that the high-symmetry point P (D_2) is *always* a Dirac point as long as the symmetries are preserved. This *model independent* Dirac point deserves some detailed analysis given below. The three screw rotations $R_{x,y,z}$ and PT are elements of the little group at P. It is straightforward to check that

$$[iR_i, iR_j] = \pm 2i\epsilon_{ijk}R_k, \quad (7)$$

forming an SU(2) group, where the lowest dimension of irreducible representations is two. On the other hand, PT requires that all iR_i are real, which is incompatible with the two dimensional representation, since $i\sigma_{x,z}$ are purely imaginary. Therefore the lowest irreducible representation is four dimensional, where $iR_{x,z} = i\sigma_{x,z} \otimes \sigma_y$ and $R_y = \sigma_y \otimes \sigma_0$. Above is the formal proof that P must be a Dirac point as long as two twofold screw axes and PT are preserved.

IV. TOPOLOGICAL SURFACE STATES WITH “DOUBLE-ARCS”

Due to the widely acknowledged bulk-edge correspondence principle, bulk topological states in d -dimensions have anomalous surface states that cannot be realized on a $d - 1$ -dimensional lattice without breaking certain symmetries. For topological band crossings, the surface bands form a helicoid structure surrounding the projection of the bulk node. To be specific, if two bulk bands cross each other at a Dirac point, then in the surface Brillouin zone, inside the gap between the two bands, there are surface states, and the dispersion of the surface states form a double-helicoid (two helicoids winding in different directions) centered at the projection of the Dirac point. As stated in Ref.[17], the equal energy contours of a double-helicoid are two arcs emanating from the Dirac point projection, ending at the projection of another Dirac point of opposite charge.

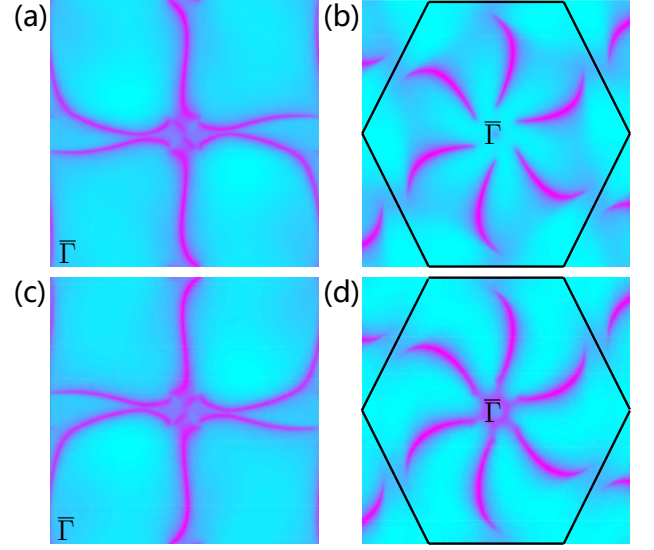


FIG. 3. The average (over all Brillouin zones) structure factor $S(\mathbf{q}, \omega)$ on the (001)- and the (111)-surface at $E = 1.436J_1$ in (a, b) for the spin flip $\delta S = +1$ and (c, d) for $\delta S = -1$, respectively.

We consider two typical open surfaces of the (001)-plane and the (111)-plane. For the (001)- and (111)-surfaces, the surface Brillouin zones are shown in Fig. 2(b) by projecting the bulk Brillouin zone. The Dirac points are also projected onto the surface Brillouin zone and there are instances when two Dirac points in the bulk Brillouin zone project to the same point on the surface. We set the parameters to $J_2 = 0.134J_1$ such that $W_{1,2,3}$ are close in energy. Then we choose an energy E_0 that is the average energy of $D_{1,2,3}$ and plot the equal energy contours in the surface Brillouin zone. For clarity, we separately plot the contribution from H_+ and H_- in Fig. 3. In a spin-unpolarized experiment, the two patterns (upper and lower) should be superimposed. We see that the projection of each positive Dirac point is connected to that of a negative Dirac point by an arc and vice versa; and the projection of two positive Dirac points is connected to the two projections of negative Dirac points and vice versa. Since the positive and negative Dirac points are set far apart in the Brillouin zone, the arcs connecting their projections are long, a desirable feature for experimental observation. Additionally, we note that due to the symmetry PT , the two opposite surfaces have identical dispersions of the surface states.

V. DISCUSSION

Finally, we remark on possible experiments that will be able to justify our assumptions and testify our predictions. The actual symmetry and configuration of the ordered phase may be better confirmed than was done using powder sample by performing elastic neutron scattering

on single crystals⁴⁰. The Dirac points as well as nodal lines in the bulk can be directly measured with inelastic neutron scattering, and they are further expected to exhibit gap-opening behaviors in a magnetic field. Since magnons of each spin form many Weyl points, there are thermal Hall currents for each spin component. However, because the total Hall current of magnons must vanish due to PT , a spin-resolved measurement of the magnon currents is required to observe this effect. The arcs states, however interesting, are expected to be difficult to directly observe by inelastic neutron scattering due to the very small sample volume from the surfaces. One may be able to detect these states using surface-sensitive probes, such as high-resolution electron energy loss spectroscopy, or helium atom energy loss spectroscopy.

ACKNOWLEDGMENTS

We wish to thank Ji Feng, Fa Wang, Xuetao Zhu and Ling Lu for discussions and Weiliang Yao for assistance

in checking some of our early calculations. The work at Institute of Physics was supported by the National Key Research and Development Program of China under grant No. 2016YFA0302400, by NSFC under grant No. 11674370, 1190020, 11534014, 11334012, by the Ministry of Science and Technology of China 973 program (Grant No. 2015CB921300), and by the Strategic Priority Research Program of CAS (Grant No. XDB07000000). The work at Peking University was supported by the National Natural Science Foundation of China (Grants No. 11374024 and No. 11522429) and Ministry of Science and Technology of China (Grants No. 2015CB921302 and No. 2013CB921903).

a

* These authors contributed equally to this study.

† yuan.li@pku.edu.cn

‡ cfang@iphy.ac.cn

¹ S. Murakami, New Journal of Physics **9**, 356 (2007).

² X. Wan, A. M. Turner, A. Vishwanath, and S. Y. Savrasov, Phys. Rev. B **83**, 205101 (2011).

³ B. Q. Lv, H. M. Weng, B. B. Fu, X. P. Wang, H. Miao, J. Ma, P. Richard, X. C. Huang, L. X. Zhao, G. F. Chen, Z. Fang, X. Dai, T. Qian, and H. Ding, Phys. Rev. X **5**, 031013 (2015).

⁴ S.-Y. Xu, I. Belopolski, N. Alidoust, M. Neupane, C. Zhang, R. Sankar, S.-M. Huang, C.-C. Lee, G. Chang, B. Wang, G. Bian, H. Zheng, D. S. Sanchez, F. Chou, H. Lin, S. Jia, and M. Z. Hasan, Science **349**, 613 (2015).

⁵ L. Lu, Z. Wang, D. Ye, L. Ran, L. Fu, J. D. Joannopoulos, and M. Soljacic, Science **349**, 622 (2015).

⁶ A. A. Burkov, Nat Mater **15**, 1145 (2016).

⁷ F. D. M. Haldane and S. Raghu, Phys. Rev. Lett. **100**, 013904 (2008).

⁸ L. Lu, J. D. Joannopoulos, and M. Soljacic, Nat Photon **8**, 821 (2014).

⁹ S. D. Huber, Nat Phys **12**, 621 (2016).

¹⁰ L. Lu, L. Fu, J. D. Joannopoulos, and M. Soljacic, Nature Photonics (2013).

¹¹ O. Stenull, C. L. Kane, and T. C. Lubensky, Phys. Rev. Lett. **117**, 068001 (2016).

¹² F.-Y. Li, Y.-D. Li, Y. B. Kim, L. Balents, Y. Yu, and G. Chen, Nature Communications **7**, 12691 EP (2016).

¹³ S. M. Young, S. Zaheer, J. C. Y. Teo, C. L. Kane, E. J. Mele, and A. M. Rappe, Phys. Rev. Lett. **108**, 140405 (2012).

¹⁴ Z. Wang, Y. Sun, X.-Q. Chen, C. Franchini, G. Xu, H. Weng, X. Dai, and Z. Fang, Phys. Rev. B **85**, 195320 (2012).

¹⁵ Z. Wang, H. Weng, Q. Wu, X. Dai, and Z. Fang, Phys. Rev. B **88**, 125427 (2013).

¹⁶ B.-J. Yang and N. Nagaosa, Nature Communications **5**, 4898 EP (2014).

¹⁷ C. Fang, L. Lu, J. Liu, and L. Fu, Nat Phys **12**, 936 (2016).

¹⁸ B. Bradlyn, J. Cano, Z. Wang, M. G. Vergniory, C. Felser, R. J. Cava, and B. A. Bernevig, Science **353** (2016), 10.1126/science.aaf5037, <http://science.sciencemag.org/content/353/6299/aaf5037.full.pdf>.

¹⁹ H. Weng, C. Fang, Z. Fang, and X. Dai, Phys. Rev. B **93**, 241202 (2016).

²⁰ Z. Zhu, G. W. Winkler, Q. Wu, J. Li, and A. A. Soluyanov, Phys. Rev. X **6**, 031003 (2016).

²¹ G. Chang, S.-Y. Xu, S.-M. Huang, D. S. Sanchez, C.-H. Hsu, G. Bian, Z.-M. Yu, I. Belopolski, N. Alidoust, H. Zheng, T.-R. Chang, H.-T. Jeng, S. A. Yang, T. Neupert, H. Lin, and M. Z. Hasan, arXiv:1605.06831v1 (2016).

²² B.-J. Yang, T. A. Bojesen, T. Morimoto, and A. Furusaki, Phys. Rev. B **95**, 075135 (2017).

²³ H. Watanabe, H. C. Po, A. Vishwanath, and M. P. Zaletel, Proc. Natl. Acad. Sci. **112** (2015).

²⁴ H. Watanabe, H. C. Po, M. P. Zaletel, and A. Vishwanath, Phys. Rev. Lett. **117**, 096404 (2016).

²⁵ C. J. BRADLEY and B. L. DAVIES, Rev. Mod. Phys. **40**, 359 (1968).

²⁶ S.-Y. Xu, C. Liu, S. K. Kushwaha, R. Sankar, J. W. Krizan, I. Belopolski, M. Neupane, G. Bian, N. Alidoust, T.-R. Chang, et al., Science **347**, 294 (2015).

²⁷ I. Dzyaloshinsky, Journal of Physics and Chemistry of Solids **4**, 241 (1958).

²⁸ T. Moriya, Phys. Rev. **120**, 91 (1960).

²⁹ C. Fang, Y. Chen, H.-Y. Kee, and L. Fu, Phys. Rev. B **92**, 081201 (2015).

³⁰ A. A. Burkov, M. D. Hook, and L. Balents, Phys. Rev. B **84**, 235126 (2011).

³¹ G. Xu, H. Weng, Z. Wang, X. Dai, and Z. Fang, Phys. Rev. Lett. **107**, 186806 (2011).

- ³² G. E. Volovik, *Journal of Superconductivity and Novel Magnetism* **26**, 2887 (2013).
- ³³ Y. Kim, B. J. Wieder, C. L. Kane, and A. M. Rappe, *Phys. Rev. Lett.* **115**, 036806 (2015).
- ³⁴ C. Fang, H. Weng, X. Dai, and Z. Fang, *Chinese Physics B* **25**, 117106 (2016).
- ³⁵ M. Herak, H. Berger, M. Prester, M. Miljak, I. Ivkovi, O. Milat, D. Drobac, S. Popovi, and O. Zaharko, *Journal of Physics: Condensed Matter* **17**, 7667 (2005).
- ³⁶ K. Y. Choi, P. Lemmens, E. S. Choi, and H. Berger, *Journal of Physics: Condensed Matter* **20**, 505214 (2008).
- ³⁷ M. Mnsson, K. Pra, J. Sugiyama, D. Andreica, H. Luetkens, and H. Berger, *Physics Procedia* **30**, 142 (2012).
- ³⁸ E. N. Maslen, V. A. Streltsov, and N. Ishizawa, *Acta Crystallographica Section B* **52**, 414 (1996).
- ³⁹ B. Antic, M. Mitric, and D. Rodic, *Journal of Magnetism and Magnetic Materials* **145**, 349 (1995).
- ⁴⁰ Z. He and M. Itoh, *Journal of Magnetism and Magnetic Materials* **354**, 146 (2014).

Appendix A: Spin wave Hamiltonian for Cu_3TeO_6

There are twelve spins in each Bravais lattice, and we denote them from 1-12 as in FIG. 1 in the main text. Each spin has four nearest neighbors (NN) and four next nearest neighbors (NNN), then it is convenient to write down the spin wave Hamiltonian for nearest neighbors and next nearest neighbors respectively, with the form of $H = H_{NN} + H_{NNN}$. Start from the Heisenberg Hamiltonian in the main text, and after Holstein-Primakoff transformation (only keep quadratic terms), the nearest neighbor spin interaction terms have the general form:

$$J_1 S_i \cdot S_j = J_1 S(a_i^\dagger a_i + a_j^\dagger a_j + a_i a_j + a_i^\dagger a_j^\dagger), \quad (\text{A1})$$

while the next nearest neighbor ones have the form:

$$J_2 S_i \cdot S_j = J_2 S(-a_i^\dagger a_i - a_j^\dagger a_j + a_i^\dagger a_j + a_i a_j^\dagger). \quad (\text{A2})$$

For nearest neighbors, there are totally twelve bond vectors, which are:

$$\begin{aligned} \delta_1 = (-f_1, -f_2, f_3), \delta_2 = (f_3, -f_1, -f_2), \delta_3 = (-f_1, f_2, -f_3), \delta_4 = (f_3, f_1, f_2), \delta_5 = (f_2, -f_3, f_1), \delta_6 = (-f_2, f_3, f_1), \\ \delta_7 = (-f_1, -f_2, -f_3), \delta_8 = (f_2, f_3, f_1), \delta_9 = (-f_3, -f_1, f_2), \delta_{10} = (-f_1, f_2, f_3), \delta_{11} = (f_2, f_3, -f_1), \delta_{12} = (-f_3, f_1, -f_2), \end{aligned}$$

where f_1, f_2, f_3, f_4 are lattice parameters and only two of them are independent with relationships as below:

$$f_2 = f_1 + f_3, f_4 = f_1 + f_2. \quad (\text{A3})$$

Take spin 1 for example, its four nearest neighbor spins are spin 2, 6, 7, 11, with bond vectors $\delta_1, \delta_2, \delta_3, \delta_4$ respectively, then after Fourier transformation, the contribution of spin 1 to the nearest neighbor part of spin wave Hamiltonian is:

$$\begin{aligned} J_1 S \sum_k (a_{1k}^\dagger a_{1k} + a_{2k}^\dagger a_{2k} + a_{1k} a_{2,-k} e^{-ik \cdot \delta_1} + a_{1k}^\dagger a_{2,-k}^\dagger e^{ik \cdot \delta_1} + a_{1k}^\dagger a_{1k} + a_{6k}^\dagger a_{6k} + a_{1k} a_{6,-k} e^{-ik \cdot \delta_2} + a_{1k}^\dagger a_{6,-k}^\dagger e^{ik \cdot \delta_2} \\ + a_{1k}^\dagger a_{1k} + a_{7k}^\dagger a_{7k} + a_{1k} a_{7,-k} e^{-ik \cdot \delta_3} + a_{1k}^\dagger a_{7,-k}^\dagger e^{ik \cdot \delta_3} + a_{1k}^\dagger a_{1k} + a_{11k}^\dagger a_{11k} + a_{1k} a_{11,-k} e^{-ik \cdot \delta_4} + a_{1k}^\dagger a_{11,-k}^\dagger e^{ik \cdot \delta_4}). \end{aligned} \quad (\text{A4})$$

For simplicity, we abbreviate it as:

$$J_1 S \sum_k ((1, 2, \delta_1) + (1, 6, \delta_2) + (1, 7, \delta_3) + (1, 11, \delta_4)). \quad (\text{A5})$$

Then the spin wave Hamiltonian of nearest neighbors can be written as:

$$\begin{aligned} H_{NN} = \frac{1}{2} J_1 S \sum_k ((1, 2, \delta_1) + (1, 6, \delta_2) + (1, 7, \delta_3) + (1, 11, \delta_4) + (2, 1, -\delta_1) + (2, 3, \delta_5) + (2, 8, \delta_6) + (2, 12, \delta_7) \\ + (3, 2, -\delta_5) + (3, 4, \delta_2) + (3, 7, \delta_8) + (3, 9, \delta_9) + (4, 3, -\delta_2) + (4, 5, -\delta_1) + (4, 8, -\delta_4) + (4, 10, -\delta_3) \\ + (5, 4, \delta_1) + (5, 6, -\delta_5) + (5, 9, -\delta_7) + (5, 11, -\delta_6) + (6, 1, -\delta_2) + (6, 5, \delta_5) + (6, 10, -\delta_8) + (6, 12, -\delta_9) \\ + (7, 1, -\delta_3) + (7, 3, -\delta_8) + (7, 8, \delta_{11}) + (7, 12, \delta_{10}) + (8, 2, -\delta_6) + (8, 4, \delta_4) + (8, 7, -\delta_{11}) + (8, 9, \delta_{12}) \\ + (9, 3, -\delta_9) + (9, 5, \delta_7) + (9, 8, -\delta_{12}) + (9, 10, \delta_{10}) + (10, 4, \delta_3) + (10, 6, \delta_8) + (10, 9, -\delta_{10}) + (10, 11, -\delta_{11}) \\ + (11, 1, -\delta_4) + (11, 5, \delta_6) + (11, 10, \delta_{11}) + (11, 12, -\delta_{12}) + (12, 2, -\delta_7) + (12, 6, \delta_9) + (12, 7, -\delta_{10}) + (12, 11, \delta_{12})), \end{aligned} \quad (\text{A6})$$

where the factor $\frac{1}{2}$ comes from the repeat count of each spin. After simple simplification, we get:

$$H_{NN} = J_1 S \sum_k \left(4 \sum_{i=1}^{12} a_{ik}^\dagger a_{ik} + ((1, 2, \delta_1) + (1, 6, \delta_2) + (1, 7, \delta_3) + (1, 11, \delta_4) + (2, 3, \delta_5) + (2, 8, \delta_6) + (2, 12, \delta_7) + (3, 4, \delta_2) \right. \\ \left. + (3, 7, \delta_8) + (3, 9, \delta_9) + (4, 5, -\delta_1) + (4, 8, -\delta_4) + (4, 10, -\delta_3) + (5, 6, -\delta_5) + (5, 9, -\delta_7) + (5, 11, -\delta_6) \right. \\ \left. + (6, 10, -\delta_8) + (6, 12, -\delta_9) + (7, 8, \delta_{11}) + (7, 12, \delta_{10}) + (8, 9, \delta_{12}) + (9, 10, \delta_{10}) + (10, 11, -\delta_{11}) + (11, 12, -\delta_{12})) + h.c. \right), \quad (A7)$$

here, the abbreviation denote, take $(1, 2, \delta_1)$ for example, $a_{1,-k} a_{2k} e^{ik \cdot \delta_1}$.

Similarly, there are also twelve next nearest neighbor bond vectors, which are:

$$\Delta_1 = (-f_4, -f_1, f_2), \Delta_2 = (-f_4, f_1, -f_2), \Delta_3 = (-f_1, f_2, f_4), \Delta_4 = (-f_1, -f_2, -f_4), \Delta_5 = (f_1, -f_2, f_4), \Delta_6 = (f_2, f_4, f_1), \\ \Delta_7 = (-f_2, -f_4, f_1), \Delta_8 = (f_2, -f_4, -f_1), \Delta_9 = (-f_4, -f_1, -f_2), \Delta_{10} = (-f_2, f_4, -f_1), \Delta_{11} = (f_1, f_2, -f_4), \Delta_{12} = (-f_4, f_1, f_2).$$

And the spin wave Hamiltonian of next nearest neighbors can be written as:

$$H_{NNN} = \frac{1}{2} J_2 S \sum_k \left(((1, 3, \Delta_2) + (1, 5, \Delta_3) + (1, 8, \Delta_1) + (1, 10, \Delta_4) + (2, 4, \Delta_3) + (2, 6, \Delta_7) + (2, 9, \Delta_5) + (2, 11, \Delta_6) \right. \\ \left. + (3, 1, -\Delta_2) + (3, 5, \Delta_7) + (3, 10, \Delta_8) + (3, 12, \Delta_9) + (4, 2, -\Delta_3) + (4, 6, -\Delta_2) + (4, 7, -\Delta_4) + (4, 11, -\Delta_1) \right. \\ \left. + (5, 1, -\Delta_3) + (5, 3, -\Delta_7) + (5, 8, -\Delta_6) + (5, 12, -\Delta_5) + (6, 2, -\Delta_7) + (6, 4, \Delta_2) + (6, 7, -\Delta_8) + (6, 9, -\Delta_9) \right. \\ \left. + (7, 4, \Delta_4) + (7, 6, \Delta_8) + (7, 9, \Delta_{11}) + (7, 11, \Delta_{10}) + (8, 1, -\Delta_1) + (8, 5, \Delta_6) + (8, 10, \Delta_{10}) + (8, 12, \Delta_{12}) \right. \\ \left. + (9, 2, -\Delta_5) + (9, 6, \Delta_9) + (9, 7, -\Delta_{11}) + (9, 11, \Delta_{12}) + (10, 1, -\Delta_4) + (10, 3, -\Delta_8) + (10, 8, -\Delta_{10}) + (10, 12, -\Delta_{11}) \right. \\ \left. + (11, 2, -\Delta_6) + (11, 4, \Delta_1) + (11, 7, -\Delta_{10}) + (11, 9, -\Delta_{12}) + (12, 3, -\Delta_9) + (12, 5, \Delta_5) + (12, 8, -\Delta_{12}) + (12, 10, \Delta_{11})) \right), \quad (A8)$$

where the factor $\frac{1}{2}$ also comes from the repeat count of each spin, and the abbreviation here denote, take $(1, 3, \Delta_2)$ for example, $(-a_{1k}^\dagger a_{1k} - a_{3k}^\dagger a_{3k} + a_{1k}^\dagger a_{3k} e^{ik \cdot \Delta_2} + a_{1k} a_{3k}^\dagger e^{-ik \cdot \Delta_2})$. After simple simplification, we get:

$$H_{NNN} = J_2 S \sum_k \left(-4 \sum_{i=1}^{12} a_{ik}^\dagger a_{ik} + ((1, 3, \Delta_2) + (1, 5, \Delta_3) + (1, 8, \Delta_1) + (1, 10, \Delta_4) + (2, 4, \Delta_3) + (2, 6, \Delta_7) \right. \\ \left. + (2, 9, \Delta_5) + (2, 11, \Delta_6) + (3, 5, \Delta_7) + (3, 10, \Delta_8) + (3, 12, \Delta_9) + (4, 6, -\Delta_2) \right. \\ \left. + (4, 7, -\Delta_4) + (4, 11, -\Delta_1) + (5, 8, -\Delta_6) + (5, 12, -\Delta_5) + (6, 7, -\Delta_8) + (6, 9, -\Delta_9) \right. \\ \left. + (7, 9, \Delta_{11}) + (7, 11, \Delta_{10}) + (8, 10, \Delta_{10}) + (8, 12, \Delta_{12}) + (9, 11, \Delta_{12}) + (10, 12, -\Delta_{11})) + h.c. \right), \quad (A9)$$

here, the abbreviation denote, take $(1, 3, \Delta_2)$ for example, $a_{1k}^\dagger a_{3k} e^{ik \cdot \Delta_2}$.

Finally, in the basis of $\Psi^\dagger(k) = (a_{1k}^\dagger, a_{2k}^\dagger, a_{3k}^\dagger, a_{4k}^\dagger, a_{5k}^\dagger, a_{6k}^\dagger, a_{7k}^\dagger, a_{8k}^\dagger, a_{9k}^\dagger, a_{10k}^\dagger, a_{11k}^\dagger, a_{12k}^\dagger, a_{1,-k}, a_{2,-k}, a_{3,-k}, a_{4,-k}, a_{5,-k}, a_{6,-k}, a_{7,-k}, a_{8,-k}, a_{9,-k}, a_{10,-k}, a_{11,-k}, a_{12,-k})$, we have:

$$H = H_{NN} + H_{NNN} = \sum_k \Psi^\dagger(k) \begin{pmatrix} A(k) & B^\dagger(k) \\ B(k) & 0 \end{pmatrix} S \Psi(k) = \frac{1}{2} \sum_k \Psi^\dagger(k) \begin{pmatrix} A(k) & 2B^\dagger(k) \\ 2B(k) & A(k) \end{pmatrix} S \Psi(k) = \frac{1}{2} \sum_k \Psi^\dagger(k) h(k) \Psi(k), \quad (A10)$$

where $h(k)$ is the spin wave Hamiltonian matrix, and the entries of $A(k)$ are:

$$A_{ii} = 4(J_1 - J_2), (i = 1 - 12), A_{13} = J_2 e^{ik \cdot \Delta_2}, A_{15} = J_2 e^{ik \cdot \Delta_3}, A_{18} = J_2 e^{ik \cdot \Delta_1}, A_{1,10} = J_2 e^{ik \cdot \Delta_4}, A_{24} = J_2 e^{ik \cdot \Delta_3}, A_{26} = J_2 e^{ik \cdot \Delta_7}, \\ A_{29} = J_2 e^{ik \cdot \Delta_5}, A_{2,11} = J_2 e^{ik \cdot \Delta_6}, A_{35} = J_2 e^{ik \cdot \Delta_7}, A_{3,10} = J_2 e^{ik \cdot \Delta_8}, A_{3,12} = J_2 e^{ik \cdot \Delta_9}, A_{46} = J_2 e^{-ik \cdot \Delta_2}, \\ A_{47} = J_2 e^{-ik \cdot \Delta_4}, A_{4,11} = J_2 e^{-ik \cdot \Delta_1}, A_{58} = J_2 e^{-ik \cdot \Delta_6}, A_{5,12} = J_2 e^{-ik \cdot \Delta_5}, A_{67} = J_2 e^{-ik \cdot \Delta_8}, A_{69} = J_2 e^{-ik \cdot \Delta_9}, \\ A_{79} = J_2 e^{ik \cdot \Delta_{11}}, A_{7,11} = J_2 e^{ik \cdot \Delta_{10}}, A_{8,10} = J_2 e^{ik \cdot \Delta_{10}}, A_{8,12} = J_2 e^{ik \cdot \Delta_{12}}, A_{9,11} = J_2 e^{ik \cdot \Delta_{12}}, A_{10,12} = J_2 e^{-ik \cdot \Delta_{11}}, \quad (A11)$$

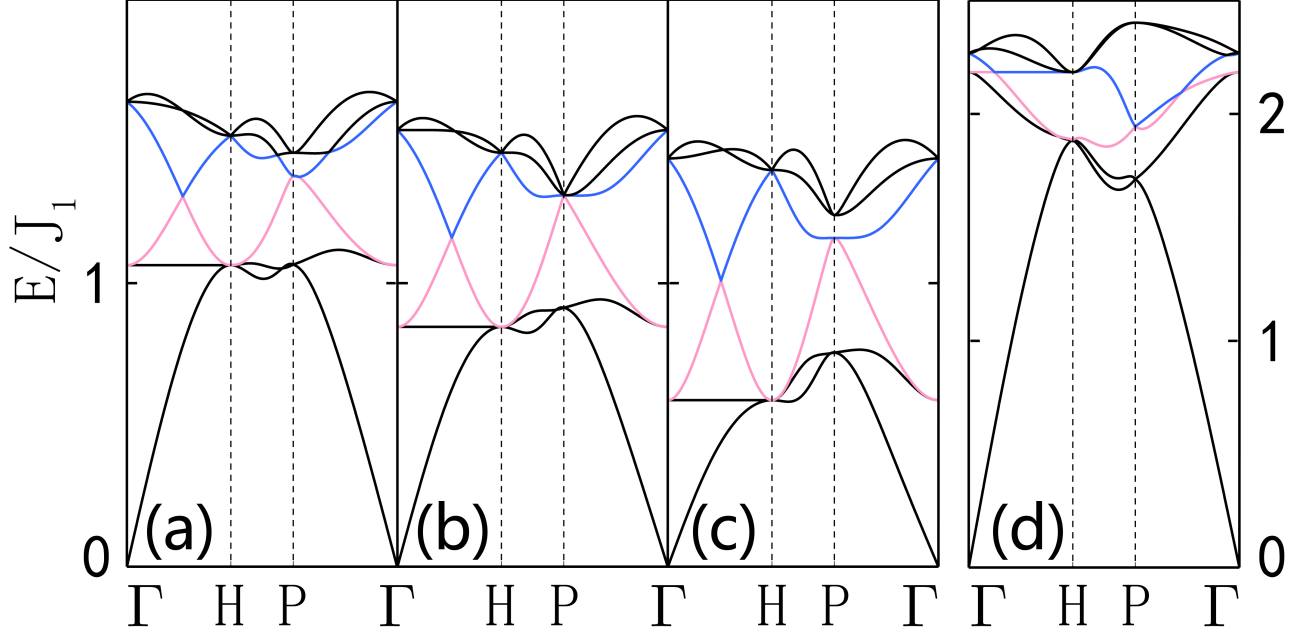


FIG. 4. The bulk band structure of the spin waves for $J_2/J_1 = 0.18, 0.23, 0.28, -0.134$, respectively.

here only upper triangular entries are shown, and the matrix can be filled by Hermitian. And the entries of $B(k)$ are:

$$\begin{aligned}
 B_{12} &= \frac{1}{2}J_1 e^{ik \cdot \delta_1}, B_{16} = \frac{1}{2}J_1 e^{ik \cdot \delta_2}, B_{17} = \frac{1}{2}J_1 e^{ik \cdot \delta_3}, B_{1,11} = \frac{1}{2}J_1 e^{ik \cdot \delta_4}, B_{23} = \frac{1}{2}J_1 e^{ik \cdot \delta_5}, B_{28} = \frac{1}{2}J_1 e^{ik \cdot \delta_6}, \\
 B_{2,12} &= \frac{1}{2}J_1 e^{ik \cdot \delta_7}, B_{34} = \frac{1}{2}J_1 e^{ik \cdot \delta_2}, B_{37} = \frac{1}{2}J_1 e^{ik \cdot \delta_8}, B_{39} = \frac{1}{2}J_1 e^{ik \cdot \delta_9}, B_{45} = \frac{1}{2}J_1 e^{-ik \cdot \delta_1}, B_{48} = \frac{1}{2}J_1 e^{-ik \cdot \delta_4}, \\
 B_{4,10} &= \frac{1}{2}J_1 e^{-ik \cdot \delta_3}, B_{56} = \frac{1}{2}J_1 e^{-ik \cdot \delta_5}, B_{59} = \frac{1}{2}J_1 e^{-ik \cdot \delta_7}, B_{5,11} = \frac{1}{2}J_1 e^{-ik \cdot \delta_6}, B_{6,10} = \frac{1}{2}J_1 e^{-ik \cdot \delta_8}, B_{6,12} = \frac{1}{2}J_1 e^{-ik \cdot \delta_9}, \\
 B_{78} &= \frac{1}{2}J_1 e^{ik \cdot \delta_{11}}, B_{7,12} = \frac{1}{2}J_1 e^{ik \cdot \delta_{10}}, B_{89} = \frac{1}{2}J_1 e^{ik \cdot \delta_{12}}, B_{9,10} = \frac{1}{2}J_1 e^{ik \cdot \delta_{10}}, B_{10,11} = \frac{1}{2}J_1 e^{-ik \cdot \delta_{11}}, B_{11,12} = \frac{1}{2}J_1 e^{-ik \cdot \delta_{12}},
 \end{aligned} \tag{A12}$$

also only the upper triangular entries are shown, however, $B(k)$ is also Hermitian in our model, and then can also be filled by Hermitian.

Appendix B: Magnon band structures at other parameters

At this point, we do not know the relative values between J_2 and J_1 except that $J_2 < J_1/3$ for the stability of the collinear antiferromagnetic ground state. In the main text, the value of $J_2 = 0.134J_1$ was chosen so that the three types of Dirac points have similar energy, optimizing the visibility of the surface arcs. In this Appendix, we show the band structures of the spin wave Hamiltonian for different $J_2/J_1 = 0.18, 0.23, 0.28, -0.134$ respectively in Fig.4.